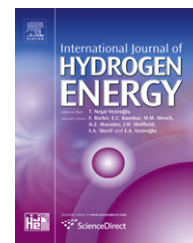


Available at [www.sciencedirect.com](http://www.sciencedirect.com)journal homepage: [www.elsevier.com/locate/he](http://www.elsevier.com/locate/he)

# The use and optimization of stainless steel mesh cathodes in microbial electrolysis cells

Yimin Zhang, Matthew D. Merrill, Bruce E. Logan\*

Department of Civil and Environmental Engineering, Penn State University, 212 Sackett Building, University Park, PA 16802, USA

## ARTICLE INFO

### Article history:

Received 15 May 2010

Received in revised form

5 August 2010

Accepted 18 August 2010

Available online 17 September 2010

### Keywords:

Stainless steel mesh

Microbial electrolysis cell

Cathode

## ABSTRACT

Microbial electrolysis cells (MECs) provide a high-yield method for producing hydrogen from renewable biomass. One challenge for commercialization of the technology is a low-cost and highly efficient cathode. Stainless steel (SS) is very inexpensive, and cathodes made of this material with high specific surface areas can achieve performance similar to carbon cathodes containing a platinum catalyst in MECs. SS mesh cathodes were examined here as a method to provide a higher surface area material than flat plate electrodes. Cyclic voltammetry tests showed that the electrochemically active surface area of certain sized mesh could be three times larger than a flat sheet. The relative performance of SS mesh in linear sweep voltammetry at low bubble coverages (low current densities) was also consistent with performance on this basis in MEC tests. The best SS mesh size (#60) in MEC tests had a relatively thick wire size (0.02 cm), a medium pore size (0.02 cm), and a specific surface area of  $66 \text{ m}^2/\text{m}^3$ . An applied voltage of 0.9 V produced a high hydrogen recovery ( $98 \pm 4\%$ ) and overall energy efficiency ( $74 \pm 4\%$ ), with a hydrogen production rate of  $2.1 \pm 0.3 \text{ m}^3\text{H}_2/\text{m}^3\text{d}$  (current density of  $8.08 \text{ A}/\text{m}^2$ , volumetric current density of  $188 \pm 19 \text{ A}/\text{m}^3$ ). These studies show that SS in mesh format shows great promise for the development of lower cost MEC systems for hydrogen production.

© 2010 Professor T. Nejat Veziroglu. Published by Elsevier Ltd. All rights reserved.

## 1. Introduction

Microbial electrolysis cells (MECs) provide a new high-yield approach for hydrogen generation from various organic substrates, such as wastewaters and other biomass. In an MEC, bacteria on the anode oxidize the organic matter and convert energy, available in a biodegradable substrate, into current. By adding a small electrical input (a minimum of 0.14 V compared to 1.23 V needed for water electrolysis) [1,2], hydrogen can be evolved on the cathode under anoxic conditions, usually with the help of a catalyst.

While many advancements in MEC performance have been made, developing a cost-effective, scalable design is the most critical challenge for the MEC to become a commercialized

hydrogen production technology [3]. Rozendal et al. [4] determined that the cathode (including catalyst) could account for the greatest percentage (47%) of the total capital costs for MECs. A precious metal such as platinum (Pt) on the cathode has been used in most studies to catalyze hydrogen evolution [3,5–7]. The disadvantages of using platinum include its high cost and poisoning by chemicals such as sulfide (a common constituent of wastewater) [3]. Several researchers have investigated new catalysts such as cobalt and iron cobalt tetramethylphenylporphyrin (CoTMPP & FeCoTMPP) [8], nickel oxide [9], stainless steel (SS) [9–11], and tungsten carbide [12]. Among these non-Pt catalysts, Ni-based alloys have demonstrated a promising electrocatalytic activity for the hydrogen evolution reaction (HER) in water electrolysis [13,14]. Hu et al.

\* Corresponding author. Tel.: +1 814 863 7908.

E-mail address: [blogan@psu.edu](mailto:blogan@psu.edu) (B.E. Logan).

0360-3199/\$ – see front matter © 2010 Professor T. Nejat Veziroglu. Published by Elsevier Ltd. All rights reserved.

doi:10.1016/j.ijhydene.2010.08.064

[15] developed NiW and NiMo catalysts by electrodepositing Ni alloys onto carbon cloth. NiMo produced hydrogen at slightly lower rates that were comparable to Pt in MECs. SS 304 with a high Ni content is cheaper and a commercially available alternative to Ni alloy. Olivares-Ramirez et al. [16] and de Souza et al. [17] reported good catalytic activation of SS 304 in an alkaline solution. In neutral pH conditions, conditions typical of MECs, Call et al. [10] obtained the highest hydrogen production rate of  $1.7 \text{ m}^3\text{H}_2/\text{m}^3\text{d}$  and overall energy efficiency of 78% using high surface area SS 304 brushes ( $650 \text{ m}^2/\text{m}^3$  of reactor volume, 0.5 cm electrode spacing) at an applied voltage of 0.6 V. This value was comparable to that obtained with a platinum-catalyzed flat carbon cloth cathode [10], indicating that expensive precious metals are not needed. However, bubble entrapment and a potentially complex construction of an MEC with brush cathodes could limit the application of this approach. In addition, careful design of the system is needed to avoid short circuiting of the SS bristles as the brush cathode must be placed in close proximity to the anode to minimize internal resistance and maximize electrode packing per volume of reactor.

In this study, we examined the use of SS mesh as alternative cathodes to flat carbon cathodes with Pt. SS mesh is flat like the carbon electrodes, allowing closer electrode spacing of the cathode to the anode, but the mesh can produce higher surface areas than a flat sheets of this metal. Mesh are characterized in terms of mesh number (number of lines of mesh per inch), with different wire diameters and pore sizes. While we expect that hydrogen evolution rates would be enhanced by surface area, bubble evolution can also be affected by pore and wire size. We therefore used linear sweep voltammetry to evaluate current densities of different mesh, and observed bubble characteristics such as coverage at different applied voltages. We also measured electrochemically active surface areas using ferrocyanide, and compared these surface areas to those estimated from mesh geometry. The mesh that had the best performance in electrochemical tests was then evaluated in MECs in terms of current densities and hydrogen production rates and recoveries.

## 2. Materials and methods

### 2.1. Cathodes

SS 304 (0.08%C, 2%Mn, 1%Si, 18–20%Cr, and 8–11%Ni [18]) woven (McMaster-Carr, IL) and expanded mesh (Dexmet Corporation, CT) were evaluated for their suitability as cathodes in MECs (Fig. 1). Mesh were cut into 3.8 cm diameter discs (projected cross sectional area of  $7 \text{ cm}^2$ ). Twelve different sized mesh (Table 1), a flat sheet of SS 304, and laboratory-made carbon cloth (type B, E-TEK; Pt,  $0.5 \text{ mg}/\text{cm}^2$ ) were examined as cathodes. Mesh characteristics are summarized in terms of wire diameter, pore size (space between adjacent wires based on the given geometry of the mesh; see Supporting information), and percent open area in Table 1. Three size ranges of SS mesh were selected for further tests in MECs based on the following characteristics: largest pore size ( $>0.04 \text{ cm}$ ; #44); thickest wire ( $\sim 0.02 \text{ cm}$ ) and medium pore

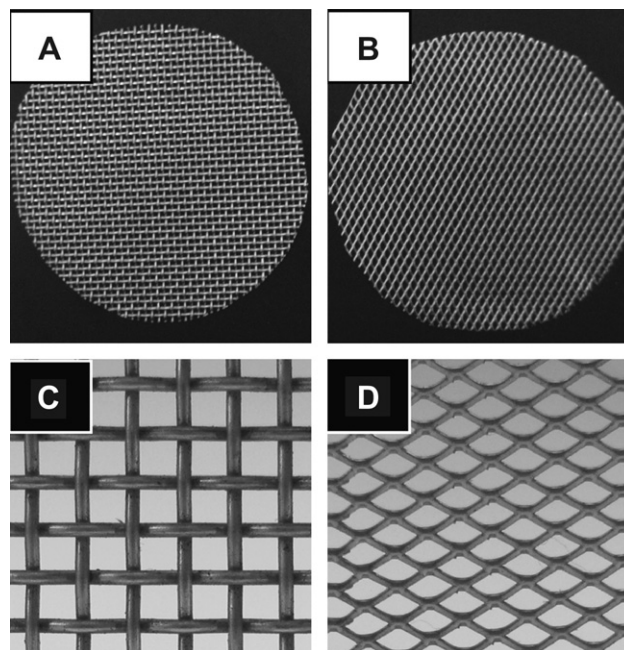


**Fig. 1 – Types of SS 304 mesh used in studies: (A) and (C) are woven mesh, (B) and (D) are expanded mesh. (A) and (B) are  $7 \text{ cm}^2$  round shape mesh, (C) and (D) are closer and magnified view of mesh structure.**

size ( $\sim 0.02 \text{ cm}$ ) (#60); and the large measured active surface area (but smallest pore sizes of  $\sim 0.01 \text{ cm}$ ; #165).

### 2.2. Electrochemical analysis

Linear sweep voltammetry (LSV) was performed on mesh using a potentiostat (model PC4/750, Gamry Instruments, Warminster, Pennsylvania) over a range of 0 V to  $-1.5 \text{ V}$  at a scan rate of  $-1 \text{ mV}/\text{s}$  ( $30 \text{ }^\circ\text{C}$ ) in a 28 mL electrochemical cell (an uninoculated MEC–reactor lacking a gas collection tube) filled with 50 mM PBS (pH = 7.04). The three electrode LSV system consisted of a working electrode (cathode electrode), counter electrode (platinum plate with a projected surface area of  $2 \text{ cm}^2$ ), and Ag/AgCl reference electrode (MF-2052, BASi, IN) (218 mV versus a standard hydrogen electrode, SHE). LSV tests were done in triplicate and the third LSV scan was used for analysis of performance based on the voltage needed to initiate hydrogen production,  $V_e$ , and the slope in the voltammogram,  $V_h$ , (Fig. 2) [8]. The first linear region was analyzed by linear regression to obtain the value of  $V_e$  and the slope  $V_h$  in the LSVs. The value of  $V_e$  indicated the relative overpotential while  $V_h$  reflects current production rate at an applied voltage. Best catalyst performance is achieved by a low  $V_e$  and large  $V_h$ . The formation of bubbles on the electrodes produces resistances which increase linearly with respect to overpotential. The effects of the mesh geometries on current densities due to bubble formation are expected to cause the differences between mesh performances. The mesh all have the same SS 304 composition and were therefore assumed to have the same hydrogen evolution activation energies. All potentials are reported versus SHE.

**Table 1 – SS meshes characteristics used in LSV and current magnitude distribution analysis.**

Mesh number	Wire diameter/cm	Pore size/cm	Open area/%	Calculated Area/cm <sup>2</sup>	Measured Area/cm <sup>2</sup>	Difference/%
flat	–	–	0	7	7	–
30	0.030	0.030	41.0	10.45	19.56	87
42	0.014	0.046	59.1	9.71	12.23	26
44	0.014	0.044	57.4	10.26	12.35	20
50	0.014	0.037	52.6	11.54	13.63	18
60	0.011	0.031	53.3	11.32	16.14	42
60	0.019	0.023	31.0	17.77	19.79	11
80	0.009	0.022	31.4	12.24	15.03	23
80	0.014	0.018	19.4	17.52	17.11	–2
90	0.014	0.015	25.4	20.15	16.96	–16
120	0.010	0.011	30.5	18.71	23.26	24
165	0.0048	0.011	47.1	12.89	18.45	43
500	0.0025	0.0025	36.0	19.30	15.54	–19

The currents for the 12 mesh at each applied voltage in LSV tests were further plotted in 3-dimensional coordinates with the z axis as current, the x axis as the wire diameter and y axis as opening size (pore size). Griddata, which is an interpolation function in Matlab, was used to define the type of surface fit to the data [19].

Active surface areas of the SS mesh were estimated by cyclic voltammetry (CV) using a ferrocyanide solution [20]. A 5 mM  $K_4Fe(CN)_6$  solution containing 0.2 M  $Na_2SO_4$  was deoxygenated with ultra high purity (UHP) nitrogen (99.998%) for 30 min and placed in same reactor used for LSV tests. The Pt/C counter electrode was wet-proofed (30%) carbon cloth (type B, E-TEK, surface area of 7 cm<sup>2</sup>, 0.5 mg/cm<sup>2</sup> Pt catalyst). The reactor was filled with solution in an anaerobic glove box to avoid oxidation of the ferrous ion. CV scans were conducted over the range of –0.3 to 1.2 V at a scan rate of 50 mV/s. The peak current,  $i_p$  (A) and effective surface area of the working electrode were obtained using the well known Matsuda's equation [20]:

$$i_p = 0.4464 \times 10^{-3} n^{3/2} F^{3/2} A (RT)^{-1/2} D_R^{1/2} C_R^* v^{1/2} \quad (1)$$

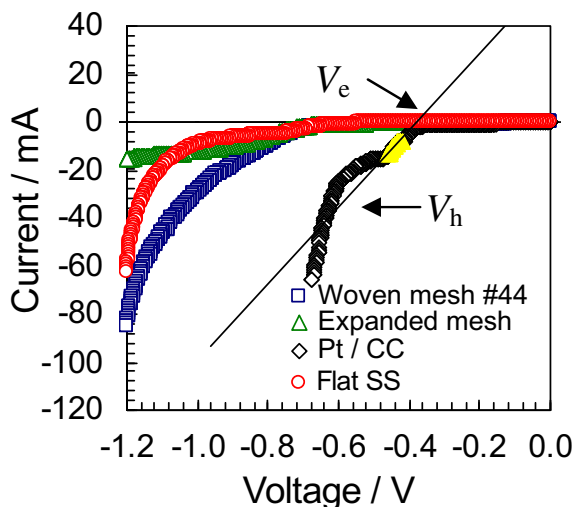


**Fig. 2 – LSV curves for the SS 304 woven mesh #44, expanded mesh, flat SS and platinum carbon cloth.**

where  $n = 1$  is the number of electrons transferred,  $F = 96487$  C/mol  $e^-$  Faraday's constant,  $R = 8.314$  J/mol K the gas constant,  $T = 303$  K the temperature,  $C_R^* = 0.005$  mol/L the initial ferrocyanide concentration, and  $v = 0.05$  V/s the scan rate. The diffusion coefficient of  $K_4Fe(CN)_6$  was calculated as  $D_R = 2.66 \times 10^{-6}$  cm<sup>2</sup>/s from the value of  $i_p$  using equation (1) and measurements for a SS flat sheet as the working electrode. Flat SS is ground then polished during the production, and thus the surface area is considered to be the same as projected area of 7 cm<sup>2</sup>. This value is comparable to that previously reported ( $6.5 \times 10^{-6}$  cm<sup>2</sup>/s; 0.1 mol L<sup>-1</sup>, 25 °C) [20]. The SS sheet was cleaned before tests using 0.5 M  $H_2SO_4$ . Based on the above given values, equation (1) becomes  $A$  (cm<sup>2</sup>) =  $2.058 \times 10^3 i_p$  (A).

### 2.3. MEC construction and operation

MECs were single-cell, cubic type reactors constructed as previously described [21]. The anode was an ammonia-treated graphite brush (25 mm diameter × 25 mm length; 0.22 m<sup>2</sup> surface area) [21] initially inoculated in single-chamber cubic MFCs with Pt/C flat cathodes [22]. The distance from the middle of brush anode to the cathode is 2.25 cm. The MFCs were fed a pre-acclimated suspension of bacteria solution (50% v/v) from an acetate-fed (1 g/L) MFC bottle-type reactor running for more than 1 year. The medium contained: 1 g/L of sodium acetate; 50 mM PBS phosphate buffer (4.58 g/L  $Na_2HPO_4$ , and 2.45 g/L  $NaH_2PO_4 \cdot H_2O$ , pH = 7.04), 0.31 g/L  $NH_4Cl$ , 0.13 g/L  $KCl$ ; and trace vitamins and minerals [22]. After a reactor reached maximum voltage for at least 3 cycles, the anode was considered acclimated and was transferred to an MEC.

MECs were operated in fed-batch mode. To avoid gas accumulation between the mesh cathode and the end plate on the top of the cylinder, a portion of the top of the mesh was cut and bent into the solution to assure no surface area loss. A power source (model 3645 A; Circuit Specialists, Inc.) was used to apply voltages ranging from 0.6 to 1.2 V. New cathodes were used for each applied voltage. The end of the batch was determined by the end of the gas production and the sharp decrease in current production. After each cycle, the reactor was drained and the electrodes were exposed to air for 20–30 min [21], refilled with substrate solution, and sparged with UHP  $N_2$  for 15 min [21]. All batch experiments were run in

**Table 2 – Correlation factors between current and SS mesh number, wire diameter, pore size, calculated surface area and measured electrochemical active area.**

		Mesh number	Wire diameter	Pore size	Calculated area	Measured area
mesh number		1.00				
wire diameter		−0.63	1.00			
pore size		−0.68	0.48	1.00		
Calculated Area		0.49	−0.29	−0.80	1.00	
Measured Area		−0.46	0.90	0.10	0.14	1.00
Current range/ mA	Cathode potential/ (V vs. SHE)					
1–10	−0.6	−0.70	0.70	0.29	0.07	0.76
	−0.7	−0.60	0.68	0.28	0.03	0.74
	−0.8	−0.68	0.68	0.36	−0.06	0.69
10–40	−0.9	−0.82	0.63	0.82	−0.48	0.42
	−1.0	−0.72	0.62	0.91	−0.57	0.33
	−1.1	−0.62	0.59	0.80	−0.43	0.36
>40	−1.2	−0.41	0.47	0.39	0.04	0.47

duplicate and maintained in a 30 °C constant temperature room. The performance of the mesh cathodes was evaluated in terms of current density, hydrogen recovery, hydrogen production rate, and the energy recovery (electrical and overall energy) as previously described [2,3].

### 3. Results

#### 3.1. Evaluation of mesh type

The minimum voltage needed to initiate substantial current ( $V_e$ ) was similar for all mesh, with  $V_e = -0.67 \pm 0.01$  V. For comparison, the Pt/CC cathode required a potential of  $-0.38$  V for current production (Fig. 2; see Table S2). Based on the mesh cathode overpotential obtained from LSVs, a minimum of 0.42 V would be required for hydrogen production in an MEC with an SS 304 mesh catalyst (assumes an anode potential of  $-0.25$  V) [2].

Woven mesh was more effective in increasing current than expanded mesh, based on higher  $V_h$  values (Fig. 2; see Table S2, Supporting information, for exact values). Woven mesh #44 and the expanded mesh possessed approximately the same wire diameter ( $\sim 0.015$  cm) and pore opening area ( $\sim 0.0025$  cm<sup>2</sup>), and therefore similar calculated surface areas (woven mesh, 9.25 cm<sup>2</sup> and expanded mesh, 8.88 cm<sup>2</sup> per 7 cm<sup>2</sup> cross sectional area). Current production was substantially lower for the expanded mesh than woven mesh at the higher current densities. The larger current per applied voltage of produced by mesh #44 could result from larger active surface areas than those calculated or different effects of structures on hydrogen bubble release and entrapment. Based on superior performance of the woven mesh, expanded mesh was not examined in further studies.

#### 3.2. Mesh characteristics

The active surface areas of the 12 different mesh were measured in CV tests (normalized to 7 cm<sup>2</sup> of cross sectional area). The electrochemically active areas measured in CV tests

for all mesh (12.23–23.26 cm<sup>2</sup>) were generally in the same range as the geometrically calculated values (9.71–20.15 cm<sup>2</sup>) (Table 1). However, there were substantial differences between values for a specific mesh. For example, mesh #30 with a relatively thick wire of 0.03 cm had an 87% larger active area than the calculated area. The largest measured surface area of 23.26 cm<sup>2</sup> obtained for Mesh #120 was three times larger than its projected surface area. Measured areas larger than those calculated from the mesh geometry could be due to underestimation of exposed areas at wire junctions, or differences in surface roughness.

The impact of mesh configuration on current was further examined through correlations between mesh number, wire diameter, pore size and surface area and LSV current densities (Table 2). In this analysis, larger correlation coefficients indicate the factor to be more relevant to variations in current generation. A negative coefficient indicates an inverse relationship between impact factor and current. While the importance of the different factors varied for different current ranges, the most significant factors overall were wire diameter and pore size. In the low current range, the wire diameter was dominant, indicated by a coefficient of 0.68–0.70. The measured active surface area was most closely related to the wire diameter (coefficient of 0.90), suggesting that wire diameter was reflective of the actual surface area. The larger active surface area, which resulted mostly from dense wire, was the most important characteristic at low current densities. In the medium current range, pore size was substantially more important (coefficient of 0.8–0.9). In the highest current range, both wire diameter and pore size were equally important. The small and negative coefficient between calculated area and current generation suggests that the areas calculated from the mesh geometry (coefficient of 0.14 between these two areas) were not a useful prediction of performance.

#### 3.3. Hydrogen evolution rates using different size mesh

At low current densities, small hydrogen bubbles at low surface coverage were observed on the different mesh (Fig. 3A). As the current increased, the bubbles expanded until

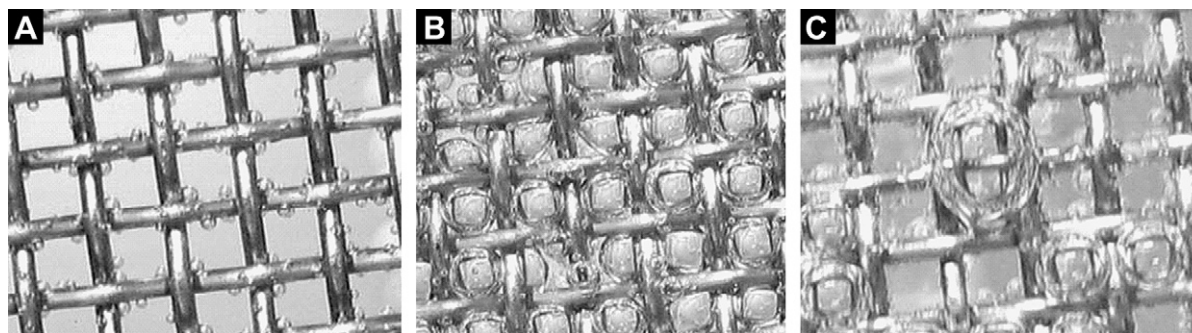


Fig. 3 – Hydrogen bubble visualization on SS mesh at 5 mA (A), 40 mA (B), 80 mA (C).

their size was essentially that of the mesh pore size, and there was high bubble coverage (Fig. 3B). At the highest current densities, the bubbles coalesced and rapidly broke away from the surface, reducing the overall bubble coverage (Fig. 3C).

To gain a better understanding of the factors affecting hydrogen evolution rate, we examined current in the three-

dimensional plots of current, wire diameter, and pore size. Current results were separated into same three ranges given above for characteristics of the bubble formation: low current, 1–10 mA; medium current, 10–40 mA; and large current, >40 mA. The magnitude of the current in each range is shown in color, with red for larger and blue for smaller currents. In the low current range, the largest currents occurred for a wire diameter between 0.02 and 0.03 cm and a pore size is between 0.02 and 0.03 cm (Fig. 4A). The largest currents were measured for mesh #60, with a wire diameter of 0.019 cm and a pore size of 0.023 cm. In the medium current range the highest currents were obtained for larger pore sizes (>0.04 cm), and similar wire diameter (0.02–0.03 cm) (Fig. 4B). Mesh #42 and #44 with the largest pore sizes therefore had the best performance. In the highest current range the optimum pore sizes were smaller (<0.03 cm) (Fig. 4C), with #60 mesh having the best performance.

To examine the optimum mesh characteristics at a relatively high ( $E_{ap} = 1.2$  V), medium ( $E_{ap} = 0.9$  V) and low currents ( $E_{ap} = 0.6$  V), #44, #60 and #165 mesh were further compared on the basis of current densities and maximum hydrogen production rates at fixed applied voltages in an electrochemical cell. The #60 mesh produced the highest current densities at the three different applied voltages, with only a slightly lower current density for the #44 mesh (Fig. 5). Mesh #165 produced  $\sim 20$ – $40$  A  $m^{-2}$  less current than the other two mesh. Mesh #60 also had the largest maximum hydrogen production rates of  $3.3 \pm 0.4$  m<sup>3</sup>H<sub>2</sub>/m<sup>3</sup>d (1.2 V),  $2.1 \pm 0.3$  m<sup>3</sup>H<sub>2</sub>/m<sup>3</sup>d (0.9 V), and  $0.8 \pm 0.1$  m<sup>3</sup>H<sub>2</sub>/m<sup>3</sup>d (0.6 V). This relative ranking of performance was in agreement with LSV studies conducted in the small current range.

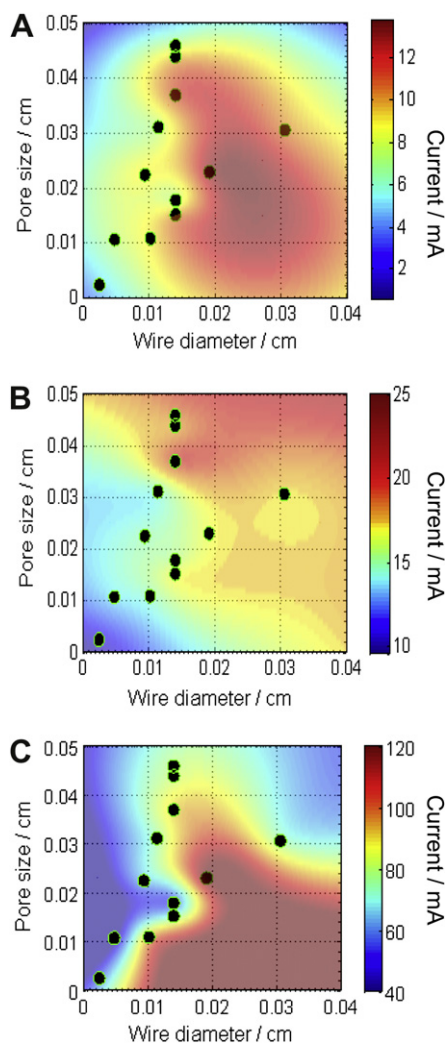


Fig. 4 – Current magnitude distribution versus mesh wire diameter and pore size at low current (A), medium current (B) and large current (C). Black dots signified each tested mesh (mesh characteristics shown in Table 1).

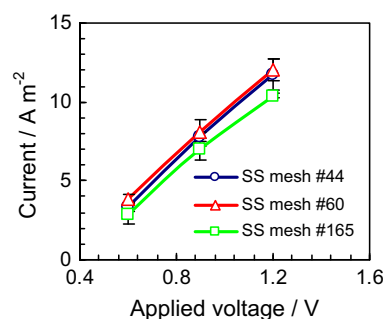
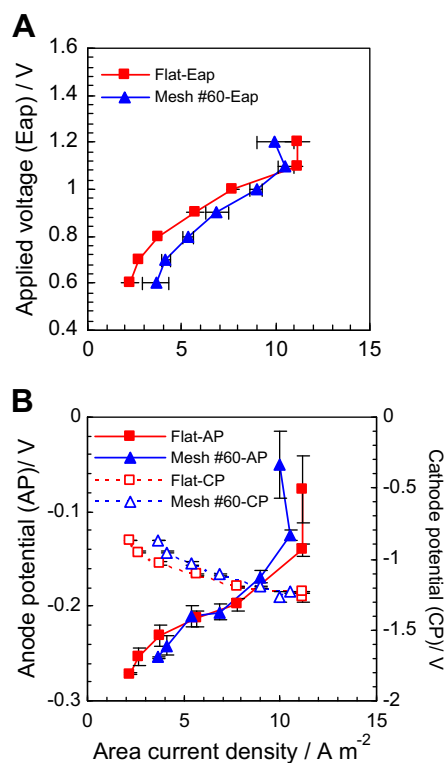


Fig. 5 – Area current densities,  $I_a$ , comparison as a function of applied voltage for SS mesh #44, #60 and #165 cathodes.



**Fig. 6** – Area current density as a function of (A) applied voltage and (B) cathode and anode potentials in MECs with flat SS or SS mesh #60 cathodes.

### 3.4. MEC tests

Flat SS as a control and mesh #60 were used in MEC tests to determine the optimum applied voltage ranging from 0.6 V to 1.2 V. The currents obtained using flat SS increased with the applied voltage from 1.6 mA (0.6 V) to 7.8 mA (1.2 V), and with mesh #60 from 2.5 mA (0.6 V) to 7.4 mA (1.1 V). The current

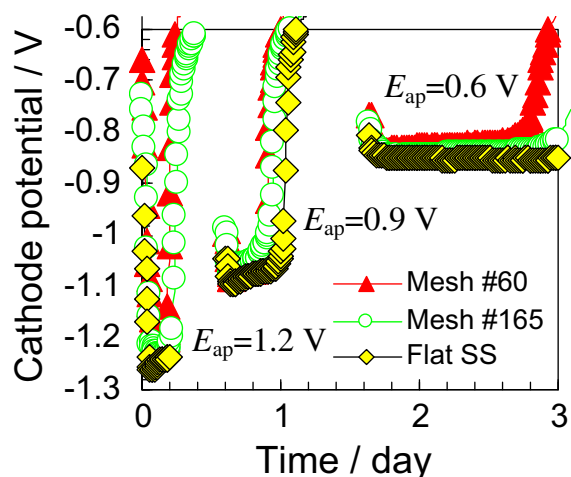


**Fig. 7** – Cathode potential versus time using flat SS and SS mesh cathodes in single-chamber MECs at  $E_{ap} = 1.2$  V, 0.9 V and 0.6 V.

**Table 3** – Comparison of meshes in terms of minimum required voltage ( $V_e$ ) by LSV and cathode potential in MECs at different applied voltage.

Mesh number	Cathode potential/V (vs. SHE)			
	LSV: $V_e$ /V	MEC		
		$E_{ap} = 0.6$ V	0.9 V	1.2 V
44	−0.68	–	–	–
60	−0.63	−0.85	−1.10	−1.22
165	−0.72	−0.86	−1.09	−1.25
Flat SS	−0.66	−0.87	−1.10	−1.27

density of flat SS was substantially lower than mesh #60 at lower applied voltage than 1.1 V (current density  $< 10$  A  $m^{-2}$ , Fig. 6A). The current-anode potential curve showed an S-shaped response (Fig. 6B), which is the typical characteristic of the electrical potential term effect on current [23]. As the applied voltage increased from 1.1 V to 1.2 V, the cathode had a relatively constant potential, while the anode potential sharply decreased from  $-0.14$  V to  $-0.076$  V for flat SS and  $-0.13$  V to  $-0.05$  V for mesh #60.

Cathode potentials measured in MEC tests showed that mesh #60, with the highest active surface area had potentials equal to or slightly more positive than the other two mesh (Fig. 7). The flat SS with the least surface area produced more negative cathode potentials than the other cathodes used in MECs. LSV tests using the same materials similarly showed that SS mesh #60, which had the highest active surface area ( $66$   $m^2/m^3$ ) and a medium pore size (0.02 cm) required the lowest applied voltage ( $V_e$ ) to start producing hydrogen (Table 3).

Coulombic efficiencies at applied voltages  $> 1.0$  V ( $E_{anode} > -0.2$  V) were lower than those obtained at voltages  $< 1.0$  V. The coulombic efficiency reached peak values at 0.8 V with  $123 \pm 4\%$  for flat SS and  $101 \pm 1\%$  for #60 mesh. CE values larger than 100% indicate electron recycling, i.e. electrons produced at the cathode being oxidized at the anode by bacteria [24].

The cathodic hydrogen recoveries ( $r_{cat}$ ) at applied voltages of 0.9–1.2 V for both cathodes were close to 100%. Hydrogen recoveries then decreased for applied voltages lower than 0.9 V because of the hydrogen losses to methane by hydro-geotrophic methanogenesis [25]. Methane was first detected

**Table 4** – Summary of MEC energy efficiencies for different mesh cathodes.

Applied Voltage/V	Mesh	$\eta_w$ /%	$\eta_{w+s}$ /%
1.2	44	$112 \pm 4$	$54 \pm 1$
	60	$138 \pm 2$	$66 \pm 3$
	165	$122 \pm 6$	$57 \pm 4$
0.9	44	$136 \pm 8$	$61 \pm 4$
	60	$173 \pm 14$	$74 \pm 4$
	165	$106 \pm 4$	$55 \pm 4$
0.6	44	$189 \pm 27$	$64 \pm 0$
	60	$232 \pm 9$	$72 \pm 11$
	165	$155 \pm 23$	$58 \pm 9$

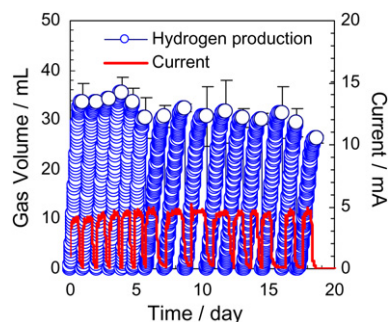


**Fig. 8 – Total gas and current production versus time with SS mesh #60 cathode at  $E_{ap} = 0.9$  V.**

at an applied voltage of 0.8 V for the flat SS, and at 0.7 V for SS #60 mesh. The current density of flat SS at lower applied voltages was substantially lower than mesh #60 (more than  $1 \text{ A m}^{-2}$ ). The flat SS MEC therefore had a longer cycle than the mesh MEC. Longer operation cycles result in greater methane production due to more time for methanogens to consume hydrogen gas [3]. The percentage of methane increased much faster for the flat mesh (from 0% to  $47.4 \pm 2.8\%$ ), than for #60 mesh (from 0% to  $4.6 \pm 1.1\%$ ) as the applied voltages decreased from 1.2 V to 0.6 V. Flat SS produced the lowest  $r_{cat} = 15 \pm 2\%$  and #60 mesh  $r_{cat} = 78 \pm 3\%$  at 0.6 V applied voltage.

The energy recovery relative to electricity input ( $\eta_w\%$ ) reached the highest value of  $232 \pm 9\%$  at 0.6 V for #60 mesh (Table 4). At 0.9 V, #60 mesh produced the highest overall energy efficiency ( $\eta_{w+s}\%$ ) of  $74 \pm 4\%$  based on both substrate and electricity input. A similar overall efficiency of  $72 \pm 11\%$  was reached at 0.6 V.

### 3.5. Corrosion

Mesh #60 was examined for possible reduction in efficiency due to corrosion by examining the stability in performance of cathodes in MEC operated for 15 cycles at an applied voltage of 0.9 V. Gas production and current densities increased slightly over the first four cycles and then stabilized at relatively constant values for the next 10 cycles. A slight decrease in gas production (below 30 mL) was observed from the 14th cycle. At the end of 15th cycle, a methane concentration of  $5 \pm 1\%$  was measured even though current was unaffected, which indicated that the decrease in gas production was not due to the mesh corrosion but rather to hydrogen conversion to methane (Fig. 8). The composition of the metal measured by SEM-EDS (Table 5) showed little

**Table 5 – Metal composition of SS mesh #60 by SEM-EDS before and after 1 month of use in MEC as cathode.**

Weight percent/%	Initial	Used
C	0.12	$0.083 \pm 0.015$
Si	0.11	$0.29 \pm 0.046$
Cr	18.39	$18.61 \pm 0.71$
Fe	72.76	$72.65 \pm 0.11$
Ni	8.62	$7.97 \pm 0.41$

variation in chromium, iron and nickel composition before and after use in MECs.

## 4. Discussion

Mesh #60, which had the densest wire packing and largest active surface area among three mesh tested in MECs ( $66 \text{ m}^2/\text{m}^3$ ) and the lowest overpotential ( $-0.63$  V) in LSV tests, achieved the highest area current densities based on projected  $7 \text{ cm}^2$  cathode area in MECs ( $12.03 \text{ A/m}^2$  at 1.2 V,  $8.08 \text{ A/m}^2$  at 0.9 V and  $3.85 \text{ A/m}^2$  at 0.6 V) and volumetric current densities normalized by  $30 \text{ cm}^3$  reactor volume ( $281 \text{ A/m}^3$  at 1.2 V,  $188 \text{ A/m}^3$  at 0.9 V and  $90 \text{ A/m}^3$  at 0.6 V). Very small mesh pores were not as effective as large pores for hydrogen gas production, likely due to entrapment of small bubbles which increased cathode overpotential. For example, #165 mesh had the highest overpotential ( $-0.72$  V) in LSV tests even though it had a relatively large active surface area ( $61 \text{ m}^2/\text{m}^3$ ). The poorer performance of #165 mesh was likely as a result of its relatively small pore size (0.01 cm) compared to #60 mesh (0.02 cm) which had a similar surface area. Cathode potentials of #165 mesh in MECs were also substantially lower than #60 mesh, especially at higher currents when bubble entrapment was observed.

Bubble coverage  $\Theta$  can be estimated from current using an empirical equation developed for horizontally placed, flat electrodes in stagnant electrolyte [26] as:

$$\Theta = 0.023 \left( \frac{I/A}{\text{A m}^{-2}} \right)^{0.23} \quad (2)$$

Bubble coverage in MECs was estimated to be  $<5\%$  based on a typical current of  $<10 \text{ mA}$ . It was visually observed during MEC tests that bubbles formed only on a small portion of the mesh and they quickly detached. Thus, only a small portion of the surface was inactivated at any time. Although large pore sizes could be useful to reduce bubble coverage, larger pores lead to smaller active surface areas. For example #44 mesh, with a pore size of 0.04 cm, has an active area of only  $41 \text{ m}^2/\text{m}^3$  and produced a 13% lower current density (0.6 V) than #60 mesh ( $66 \text{ m}^2/\text{m}^3$ , 0.02 cm pore size). The good correlation between mesh performance based on pore size and current (particularly in the medium current density range) supported our examination of the effect of bubbles on hydrogen production. At the highest current densities the rapid rate of bubble evolution creates fluid shear that helps to detach bubbles. This suggests that stirring or creating shear flow near the surface of the electrodes could enhance hydrogen evolution rate, to an extent dependent on the mesh characteristics and bubble sizes.

Although #60 mesh exhibited the best results in terms of current densities, hydrogen and energy recoveries, the current density ( $90 \pm 7 \text{ A/m}^3$ , applied voltage of 0.6 V) with  $66 \text{ m}^2/\text{m}^3$  was half that obtained with a SS brush having a much higher surface area ( $810 \text{ m}^2/\text{m}^3$ ) [12] or a carbon cloth with a Pt catalyst [21]. This suggests that greater current densities could require the use of multiple SS mesh cathodes. The SS mesh used here is flexible and therefore could be made into different configurations and perhaps placed closer to the anode in order to

reduce ohmic losses [4]. The main advantage of SS compared to other materials is its low cost. For example the purchased cost of the #60 mesh used in a single small reactor here (30 ml) is \$0.004, compared to \$0.03 for the half SS brush cathode and \$0.15 for the Pt on the Pt/C cathode [27,28]. Thus, the lower performance of the mesh could be balanced by substantially lower materials costs for larger-scale systems.

## 5. Conclusions

Stainless steel mesh, as a more scalable and low-cost cathode was first examined in MECs. The results obtained demonstrated that SS woven mesh performed better than expanded mesh as a catalyst for hydrogen evolution. The largest active surface area measured by CV reached specific area of  $78 \text{ m}^2/\text{m}^3$  (SS mesh #120), which is three times the active surface area of a flat sheet. An optimum size range existed for different current ranges and bubble coverages. Mesh wire diameter was the dominant factor of hydrogen evolution rate at low currents (<10 mA) and small bubble coverages. The wire diameter of 0.02–0.03 cm was most beneficial to the hydrogen evolution rate. Mesh pore size was dominant at medium currents (10–40 mA) and high bubble coverages. Large pore size (>0.04 cm) mesh allowed for more efficient gas evolution. At high currents (40–100 mA), mesh wire diameter and pore size were of fairly equal in importance to current generation. Higher applied voltages (>1.1 V, anode potential > -0.1 V) limited anode performance and current production rate. Low applied voltages (<0.9 V) reduced the catalytic activity and hydrogen recovery. The optimum applied voltage was 0.9 V in respect to high hydrogen recovery and overall energy efficiency. SS mesh did not show any evidence of corrosion over time in MEC tests conducted here.

## Acknowledgements

This study was supported by the King Abdullah University of Science and Technology (KAUST) (Award KUS-I1-003-13).

## Appendix. Supplementary data

Supplementary data associated with this article can be found in the online version, at doi:10.1016/j.ijhydene.2010.08.064.

## REFERENCES

- [1] J. Ivy. Summary of electrolytic hydrogen production: milestone completion report; 2004.
- [2] Logan BE. Microbial fuel cells. Hoboken, New Jersey: John Wiley & Sons, Inc.; 2008.
- [3] Logan BE, Call D, Cheng S, Hamelers HVM, Sleutels THJA, Jeremiasse AW, et al. Microbial electrolysis cells for high yield hydrogen gas production from organic matter. *Environ Sci Technol* 2008;42:8630–40.
- [4] Rozendal RA, Hamelers HVM, Rabaey K, Keller J, Buisman CJN. Towards practical implementation of bioelectrochemical wastewater treatment. *Trends Biotechnol* 2008;26:450–9.
- [5] Liu H, Grot S, Logan BE. Electrochemically assisted microbial production of hydrogen from acetate. *Environ Sci Technol* 2005;39:4317–20.
- [6] R.A. Rozendal, H.V.M. Hamelers, G.J.W. Euverink, S.J. Metz, C. J.N. Buisman, Process for producing hydrogen, WO2005005981; 2005
- [7] Rozendal RA, Hamelers HVM, Euverink GJW, Metz SJ, Buisman CJN. Principle and perspectives of hydrogen production through biocatalyzed electrolysis. *Int J Hydrogen Energy* 2006;31:1632–40.
- [8] Cheng SA, Logan BE. Evaluation of catalysts and membranes for high yield biohydrogen production via electrohydrogenesis in microbial electrolysis cells (MECs). *Water Sci Technol* 2008;58:853–7.
- [9] Selembo PA, Merrill MD, Logan BE. The use of stainless steel and nickel alloys as low-cost cathodes in microbial electrolysis cells. *J Power Sources* 2009;190:271–8.
- [10] Call DF, Merrill MD, Logan BE. High surface area stainless steel brushes as cathodes in microbial electrolysis cells. *Environ Sci Technol* 2009;43:2179–83.
- [11] Munoz LD, Benjamin E, Luc E, Julien R, Regine B, Alain B. Combining phosphate species and stainless steel cathode to enhance hydrogen evolution in microbial electrolysis cell (MEC). *Electrochem Commun* 2010;12:183–6.
- [12] Harnisch F, Schroder U, Quaas M, Scholz F. Electrocatalytic and corrosion behaviour of tungsten carbide in near-neutral pH electrolytes. *Appl Catal B Environ* 2009;87:63–9.
- [13] Navarro-Flores E, Chong ZW, Omanovic S. Characterization of Ni, NiMo, NiW and NiFe electroactive coatings as electrocatalysts for hydrogen evolution in an acidic medium. *J Mol Catal A Chem* 2005;226:179–97.
- [14] Martinez S, Metikos-Hukovic M, Valek L. Electrocatalytic properties of electrodeposited Ni-15Mo cathodes for the HER in acid solutions: synergistic electronic effect. *J Mol Catal A Chem* 2006;245:114–21.
- [15] Hu HQ, Fan YZ, Liu H. Hydrogen production in single-chamber tubular microbial electrolysis cells using non-precious-metal catalysts. *Int J Hydrogen Energy* 2009;34:8535–42.
- [16] Olivares-Ramirez JM, Campos-Cornelio ML, Godinez JU, Borja-Arco E, Castellanos RH. Studies on the hydrogen evolution reaction on different stainless steels. *Int J Hydrogen Energy* 2007;32:3170–3.
- [17] de Souza RF, Padilha JC, Goncalves RS, de Souza MO, Rault-Berthelot J. Electrochemical hydrogen production from water electrolysis using ionic liquid as electrolytes: towards the best device. *J Power Sources* 2007;164:792–8.
- [18] ASTM, Document number A 959–07, Standard guide for specifying harmonized standard grade compositions for wrought stainless steels. Table 1. Chemical Composition Limits, %; October 4, 2008
- [19] Sandwell DT. Biharmonic spline interpolation of geos-3 and seasat altimeter data. *Geophys Res Lett* 1987;14:139–42.
- [20] Bard AJ, Faulkner LR. *Electrochemical Methods: Fundamentals and Application*. New York: Wiley; 1982.
- [21] Call D, Logan BE. Hydrogen production in a single chamber microbial electrolysis cell lacking a membrane. *Environ Sci Technol* 2008;42:3401–6.
- [22] Cheng SA, Logan BE. Ammonia treatment of carbon cloth anodes to enhance power generation of microbial fuel cells. *Electrochem Commun* 2007;9:492–6.

- [23] Lee HS, Torres CI, Rittmann BE. Effects of substrate diffusion and anode potential on kinetic parameters for anode-respiring bacteria. *Environ Sci Technol* 2009;43:7571–7.
- [24] Lee HS, Torres CI, Parameswaran P, Rittmann BE. Fate of H<sub>2</sub> in an upflow single-chamber microbial electrolysis cell using a metal-catalyst-free cathode. *Environ Sci Technol* 2009;43:7971–6.
- [25] Wang AJ, Liu WZ, Cheng SA, Xing DF, Zhou JH, Logan BE. Source of methane and methods to control its formation in single chamber microbial electrolysis cells. *Int J Hydrogen Energy* 2009;34:3653–8.
- [26] Vogt H, Balzer RJ. The bubble coverage of gas-evolving electrodes in stagnant electrolytes. *Electrochim Acta* 2005;50:2073–9.
- [27] MEPS, World stainless steel prices, <http://www.meps.co.uk/Stainless%20Prices.htm>.
- [28] Kitco, 24 h platinum spot chart, <http://www.kitco.com/market/>.